Supercirculation Effects Induced by Vectoring a Partial-Span Rectangular Jet

Francis J. Capone*
NASA Langley Research Center, Hampton, Va.

Thrust-induced supercirculation effects from thrust vectoring have indicated a potential for not only increasing maneuverability of fighter aircraft but also as a means of improving cruise performance. The current study investigated a partial-span rectangular jet-exhaust nozzle located at the wing trailing edge that acts similarly to a jet flap by increasing lift due to supercirculation. This paper summarizes experimental studies including the effects of nozzle deflection angle, wing camber, and nozzle shape and exit location on lift, drag, and load distributions. The results indicate that significant increases in thrust-induced lift along with substantial decreases in drag were found. A maximum lift gain factor of 4 was achieved and thrust recovery was maintained to a lift coefficient of 0.50. Of several airfoils considered, the supercritical airfoil exhibited superior performance with respect to both lift augmentation and thrust recovery. Overall performance was maintained to a Mach number of 0.90.

Nomenclature†

$b/2$	= semispan
C_D	= drag coefficient
$C_{D,i}$	= induced drag coefficient
$C_{D,min}$	= jet-off minimum drag coefficient
$C_{(F\text{-}D)}$	= thrust-minus-drag coefficient
C_L	= aerodynamic lift coefficient, $C_{L,0}+C_{L,\Gamma}$
$C_{L,0}$	= jet-off lift coefficient
$C_{L,j}$	= measured jet lift coefficient, $C_T \sin(\alpha+\delta)$
$C_{L,\Gamma}$	= jet-induced circulation lift coefficient
ΔC_L	$= C_{L,\Gamma}+C_{L,j}$
C_m	= pitching-moment coefficient including thrust effects
C_p	= pressure coefficient
C_T	= gross-thrust coefficient
c	= chord, cm
c_r	= root chord, cm
$\bar{c}$	= average wing chord, cm
c_n	= wing section normal force coefficient
M	= freestream Mach number
$p_{t,j}/p_\infty$	= nozzle pressure ratio
x	= longitudinal distance, cm
$y/(b/2)$	= fraction of semispan
α	= angle of attack, deg
δ	= measured effective jet turning angle, deg
δ_d	= design nozzle deflection angle, deg

Introduction

ONE means for improving the maneuverability of high-performance fighter aircraft is to increase the maximum usable lift capabilities at high subsonic speeds. While considerable effort is being directed toward developing lift by aerodynamic means such as maneuver flaps or strakes, little information is available for properly evaluating the potential of propulsive lift schemes.

Exploratory studies[1,2] at the Langley Research Center have led to a proposal for vectored thrust (jet flap) concept where a rectangular jet-exhaust nozzle is located at the base of the configurations fuselage at the wing trailing-edge notch. When deflected, this jet acts much like a partial-span jet flap by increasing lift from supercirculation about the wing-body combination due to the induced flowfield associated with the deflected jet. As illustrated in Fig. 1, the total lift of this type of propulsive-lift system is composed of induced lift due to supercirculation in addition to the basic wing and jet lift. The potential advantages of this type of system can be utilized in two ways, at cruise with no increase in drag and at maneuvering conditions. This scheme permits the use of all the engine exhaust to simulate the jet flap, avoids ducting through the wing, and limits mechanical articulation to the exhaust nozzles.

This paper summarizes the transonic aerodynamic characteristics obtained from a series of parametric studies whose purpose was to provide the information necessary to properly evaluate the potential of this propulsive-lift concept for use on highly maneuverable aircraft. The scope of these studies, shown in Fig. 1, includes the effect of nozzle deflection angle, airfoil camber, and nozzle shape and exit location on lift, drag, pitch, and load distributions. A summary of the configurations tested is presented in Table 1.

Apparatus and Procedure

This investigation was conducted in the Langley 16 ft transonic tunnel[3] at Mach numbers from 0.40-0.95 over a Reynolds number range based on mean geometric chord of 2.65×10^6 to 4.13×10^6. A sketch showing the external

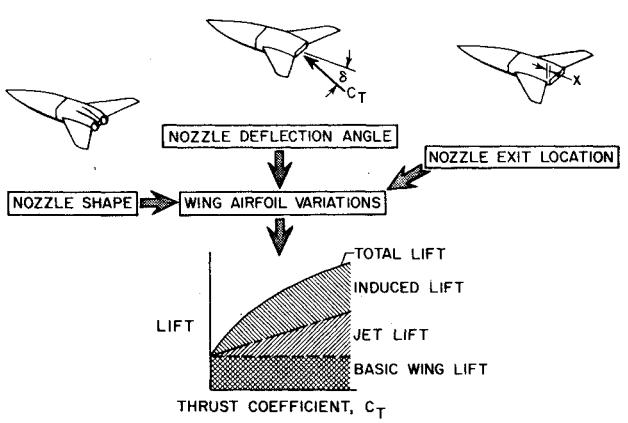

Fig. 1 Objective and scope of investigation.

Presented as Paper 74-971 at the AIAA 6th Aircraft Design, Flight Test, and Operations Meeting, Los Angeles, California, August 12-14, 1974; submitted August 26, 1974; revision received December 20, 1974.

Index categories: Aircraft Aerodynamics (including Component Aerodynamics); Aircraft Configuration Design; Aircraft Powerplant Design and Installation.

*Aerospace Engineer, High-Speed Aerodynamics Division. Member AIAA.

†All forces nondimensionalized with respect to wing reference area and freestream dynamic pressure.

Table 1 Summary of configurations tested

	Nozzle deflection effects $x/c_r=0$ δ_d				Nozzle exit location effects - 64A406 x/c_r					Flap effects 64A006 δ_f			
Wing	0	15	30	45	δ_d	0	0.07	0.14	0.21	δ_d	10	20	30
64A006	X	X	X		0	X		X		0	X	X	X
64A406	X	X	X	X	15	X	X	X	X	15	X	X	X
Supercritical 64A406	X		X		30	X		X		30	X	X	
Pressure wing 64A406 + Round nozzles	X		X		45	X		X					

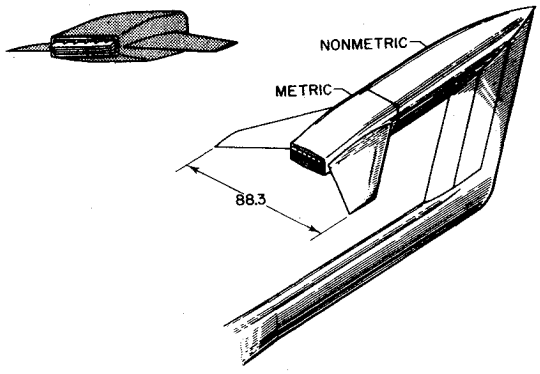

Fig. 2 Sketch of model, dimensions in centimeters.

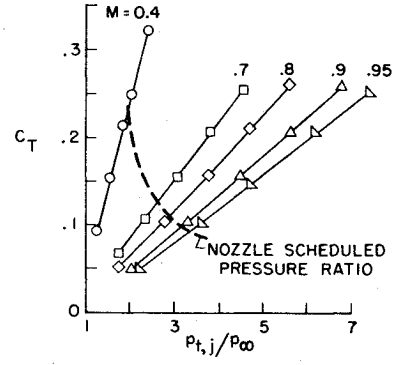

Fig. 4 Nozzle pressure ratio and Mach number test envelope.

Table 2 Wing geometric characteristics

Leading-edge sweep	50°
Aspect ratio	3
Taper ratio	0.3
Reference area, cm^2	2600
Span, cm	88.3
Mean geometric chord, cm	32.2

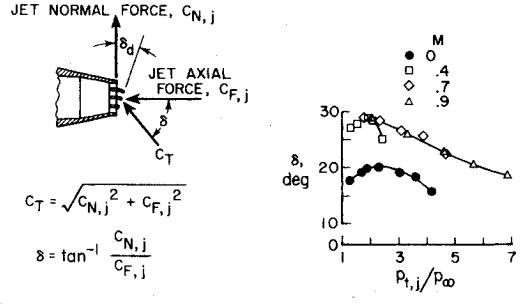

Fig. 3 Typical variation of measured turning angle with nozzle pressure ratio. $\delta_d = 30°$.

geometry and support system of the model is shown in Fig. 2. The wing geometric characteristics are given in Table 2. Boundary-layer transition strips were fixed to the model for all tests. The fuselage had rectangular cross-sections with rounded corners and an afterbody boattail angle of 12.5°.

The model had a twin-jet propulsion-simulation system with twin-bellows arrangements for eliminating transfer of axial momentum of the jet flow across the force balances. The metric system consisted of a double balance "piggyback" arrangement in which one balance measured the internal normal and axial forces on the nozzles and the second balance measured the total thrust-minus-drag forces on the entire model aft of the metric break (Fig. 2). This arrangement allowed for direct measurement of the effective jet turning angle and jet lift at all conditions.

The nozzles had rectangular exits with an exit to maximum body cross-sectional area ratio of 0.18 and an aspect ratio of 6. Jet turning was accomplished through the use of three circular arc turning vanes as shown in Fig. 3. These vanes were completely washed by the jets in order to minimize the influence of the external flow. Typical measured turning angles for the 30° nozzle are shown in Fig. 3. A significant increase in turning angle is indicated for all the wind-on cases. Similar results were found for the 15° and 45° nozzles. The test envelope of nozzle pressure ratio and freestream Mach number is indicated in Fig. 4 along with the attendant values of thrust coefficient. For simplicity, the results shown herein were obtained for the typical jet pressure ratio schedule indicated in Fig. 4 by the dashed line.

Effect of Nozzle Deflection

Lift Characteristics

The total lift due to thrust vectoring was shown in Fig. 1 to be composed of three parts.

$$\text{total lift} = C_{L,0} + C_{L,j} + C_{L,\Gamma} \tag{1}$$

where $C_{L,0}$ is the basic jet-off lift, $C_{L,j}$ is jet lift, and $C_{L,\Gamma}$ is the jet-induced supercirculation lift. To illustrate the lift characteristics of the present vectored thrust configuration, data in the form of incremental lift is presented, that is

$$\Delta C_L = C_{L,j} + C_{L,\Gamma} \tag{2}$$

where the basic jet-off lift has been subtracted from the total lift obtained from measurements of the total powered model and the jet lift $C_{L,j}$ was determined from measurements of nozzle internal forces.

Typical results showing the effects of deflecting a jet at the wing trailing edge are presented in Fig. 5. To the upper left is shown the variation of the lift increment ΔC_L with nozzle thrust coefficient for the 30° nozzle. The shaded portion of this figure is measured jet lift which is nonlinear with increasing thrust coefficient because of the decrease of effective jet turning shown previously, in Fig. 3. Also presented is a computed jet lift, $C_T \sin \delta_{\text{static}}$, based on maximum static turning.

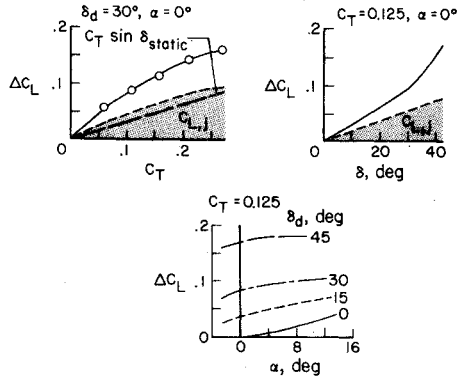

Fig. 5 Effects of varying nozzle deflection angle on incremental lift with 64A406 airfoil. $M = 0.7$.

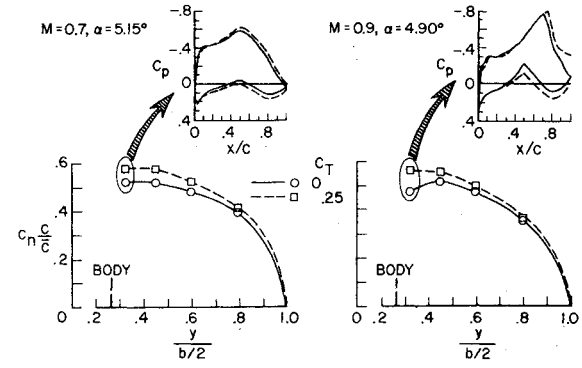

Fig. 6 Effect of thrust vectoring on chordwise and spanwise loading characteristics for 64A406 airfoil. $\delta_d = 30°$.

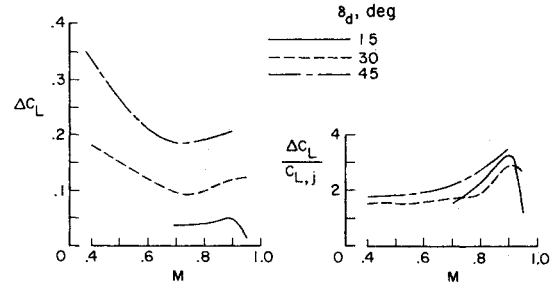

Fig. 7 Effect of Mach number on incremental lift and gain factor with 64A406 airfoil. $\alpha = 0°$ at scheduled pressure ratio.

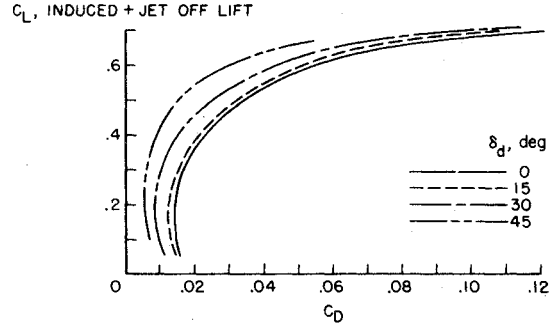

Fig. 8 Effect of nozzle deflection on drag characteristics with 64A406 airfoil. $M = 0.7$, $C_T = 0.125$.

The variation of lift increment ΔC_L with measured turning angle δ is shown in the upper right portion of Fig. 5. Data are presented at $M = 0.70$, $\alpha = 0°$, and at $C_T = 0.125$ which corresponds to the scheduled pressure ratio of Fig. 4. Lift increment varies linearly with measured turning angle up to 27°. The effects of angle of attack on the lift increment can be seen by examining the lower half of Fig. 5. For the 0° and 15° nozzles, the increase in incremental lift with increasing angle of attack is due to an increase in both jet lift and jet-induced lift. For example, half of the incremental lift for the 0° nozzle at $\alpha = 13.5°$ is induced lift. For the 30° and 45° nozzles, increases in incremental lift are due primarily to an increase in jet lift with increasing angle of attack.

In order to gain some insight into the basic flow phenomena occurring from the interaction of the deflected jet and wing flowfields, pressure distributions on the wings with the 64A406 airfoil section were measured at four span stations. Typical results illustrating subcritical conditions at $M = 0.70$ and supercritical conditions at $M = 0.90$ are presented in Fig. 6. The data shown are for jet-off and maximum thrust conditions.

At $M = 0.70$, operating the jets at the wing trailing edge is seen to increase span loading out to the tip with greater loading occurring inboard. Typical section characteristics shown in the insert indicate that at this Mach number the jet exerts a greater influence over the airfoil lower surface than over the upper surface. An examination of the wing loading characteristics at $M = 0.70$ at higher angles of attack indicates that the outboard portion of the wing becomes progressively more separated, and operating the jet at these conditions has no effect on the separated portion of the wing. By improving the flow separation characteristics of the wing at angle of attack, it is probable that the deflected jet will remain effective in inducing supercirculation lift.

At $M = 0.90$, where supersonic flow exists over a large portion of the airfoil, a smaller region of the airfoil is affected by the jet. On the top of the wing, there is a rearward shift of the shock wave (about 0.05 c) with jet operation. In general, the shock assumes this position at the initial power-on condition and further increases in nozzle pressure ratio do not alter the shock location. On the inboard lower surface ($y/(b/2) < 0.45$), the rapid expansion of the flow jet-off is reduced by the jet. Outboard on the wing lower surface ($y/(b/2) > 0.45$), the pressure distributions are similar in character to those occurring at $M = 0.70$.

The variation of incremental lift ΔC_L and lift gain factor $\Delta C_L/C_{L,j}$ with Mach number at the pressure ratio schedule for three nozzle deflections is presented in Fig. 7. For the chosen pressure ratio schedule, there is a reduction in incremental lift up to $M = 0.70$ after which ΔC_L generally increases. However, when the gain factor $\Delta C_L/C_{L,j}$ is used as a measure of the performance of the system, there is no degradation in lift augmentation with increasing Mach number except for the 15° nozzle at $M = 0.95$ and only at low thrust coefficient ($C_T < 0.12$). As shown in Fig. 7, a gain factor of 3.5 was attained for the 45° nozzle at $M = 0.90$. A maximum gain factor of 4.0 was achieved for the 64A406 wing in combination with the 45° nozzle.

Drag and Thrust Recovery

The two-dimensional jet flap has been shown to be an effective means for significantly inducing lift while at the same time recovering a part of the thrust lost due to deflecting the jet. Thrust recovery for a three-dimensional configuration at transonic speeds has already been demonstrated.[1] However, before proceeding to the thrust recovery characteristics, it is first necessary to discuss the effects of varying nozzle deflection angle on drag coefficient.

Typical drag polars for the model with the 64A406 wing are shown in Fig. 8 at $M = 0.70$. Both lift and drag coefficients are determined by subtracting measured thrust forces from the measured total powered-model forces. Lift coefficient C_L is jet-induced plus jet-off lift and represents the total aerodynamic lift of the wings. As shown, increasing nozzle deflection angle from 0 to 45° reduced the drag coefficient over the entire lift range. This reduction is due primarily to the induced upwash field created in front of the wing by the deflected jet. Consequently, at constant angle of attack, the increase in the resultant force on the wing is only in the lift direction if there is no increase in drag. An analysis of the

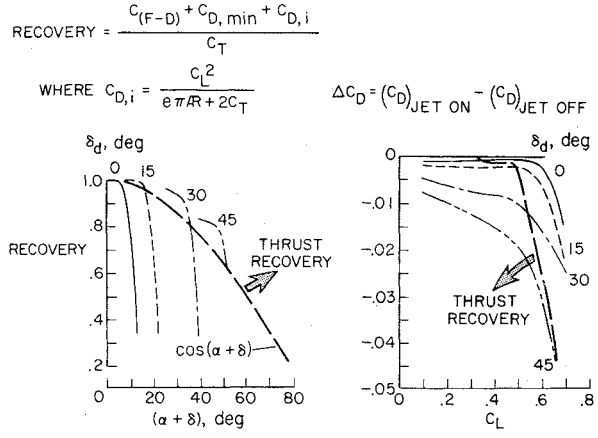

Fig. 9 Effect of nozzle deflection on thrust recovery with 64A406 airfoil at $M=0.7$, $C_T=0.125$.

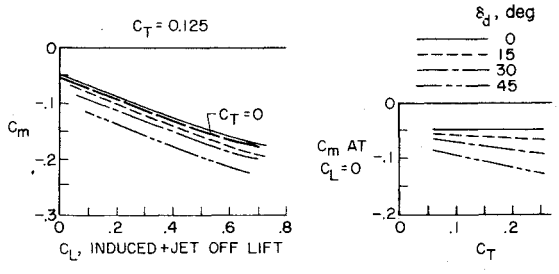

Fig. 10 Effect of nozzle deflection on pitching moment with 64A406 airfoil. $M=0.7$.

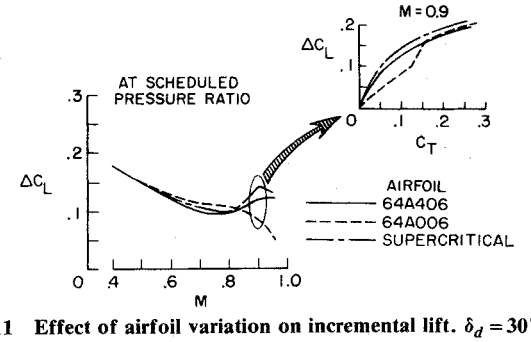

Fig. 11 Effect of airfoil variation on incremental lift. $\delta_d=30°$, $\alpha=0°$.

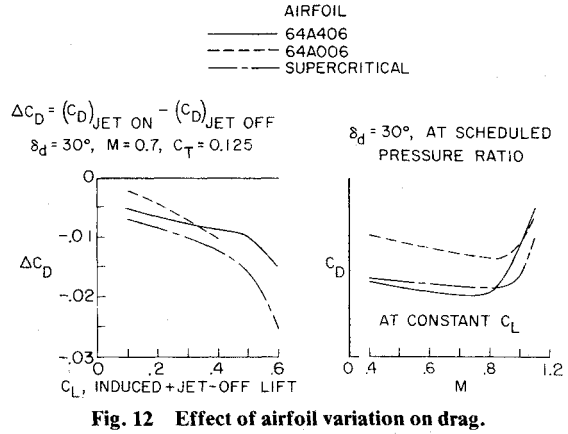

Fig. 12 Effect of airfoil variation on drag.

drag-due-to-lift characteristics of the drag polars using the method of Ref. 4 indicates that there is a reduction in drag due to lift for the 45° nozzle for most test conditions. This reduction may be attributed to improvements in leading-edge suction. A small decrease in afterbody drag generally also contributes to the overall decrease in drag coefficient.

Several methods for determining thrust recovery have been used in the past.[1,5,6] For the present study thrust recovery, which is that portion of the thrust recovered in the streamwise direction, is defined similarly to that of Ref. 5.

$$\text{recovery} = (C_{(F-D)} + C_{D,\min} + C_{D,i})/C_T \qquad (3)$$

where $C_{(F-D)}$ is thrust-minus-drag coefficients, $C_{D,\min}$ is the average jet-off minimum drag coefficient, and $C_{D,i}$ is induced drag coefficient as defined by Maskell and Spence[7] or

$$C_{D,i} = C_L^2/(e\pi AR + 2\,C_T) \qquad (4)$$

The wing efficiency factor e was also determined for jet-off conditions.

Thrust recovery as a function of $\alpha+\delta$ for the four nozzles at $M=0.70$ is presented on the left side of Fig. 9. The line of zero thrust recovery cos $(\alpha+\delta)$ is also shown. Each nozzle recovers thrust up to where viscous effects such as flow separation are developing on the wing. As deflection angle is increased, recovery in percent thrust coefficient increases from about 3% for the 15° nozzle to about 11% for the 45° nozzle. An envelope curve drawn through the points of maximum thrust recovery can serve as a guide to the operational potential of the current system. For example, these data indicate that the 15° nozzle would provide attractive improvements in cruise performance since nearly 100% thrust is recovered. Variation of thrust coefficient had little effect on thrust recovery for this nozzle.

Figure 8 showed that at constant lift coefficient, power effects decreased drag coefficient with increasing jet deflection angle. Using the average jet-off drag polar, a power drag increment can be defined as

$$\Delta C_D = (C_D)_{\text{jet on}} - (C_D)_{\text{jet off}} \qquad (5)$$

These increments are shown for $M=0.70$ to the right of Fig. 9 as a function of lift coefficient. Also shown is the line of zero thrust recovery, that is, the lift coefficient corresponding to recovery equal to cos $(\alpha+\delta)$. Note for example, that although a drag reduction of 240 counts exists for the 30° nozzle at $C_L=0.7$, this reduction could not be utilized since the wing is experiencing negative recovery (within limits imposed by definition).

Pitching-Moment Characteristics

The effects of varying nozzle deflection angle on pitching-moment characteristics are presented in Fig. 10 at $M=0.70$. Pitching moments presented include thrust effects and are referred to the quarter chord of the mean geometric chord of the wing. Pitching moment at zero lift at $M=0.7$ is also summarized as a function of nozzle thrust coefficient. Varying nozzle deflection angle affects only C_m at $C_L=0$ similar in magnitude to that caused by deflection of a trailing-edge flap. A canard most likely would trim a configuration employing this vectored-thrust system. To trim would require an upload on the canard which would increase the overall lift of the configuration.

Effect of Airfoil Shape

Lift Characteristics

Three wing sections, 64A006, 64A406, and supercritical were tested. These results are summarized in Fig. 11, where incremental lift ΔC_L is shown as a function of Mach number (at scheduled pressure ratio) for the 30° nozzle and $\alpha=0°$. There is little or no effect of airfoil shape up to $M=0.80$. Maximum lift gain factor for the supercritical wing was about 4.2.

One effect of the interaction of the deflected jet with the wing flowfield is illustrated at $M=0.90$ by the insert on Fig. 11. Here, the variation of incremental lift with thrust coefficient for the 30° nozzle at $\alpha=0°$ is shown for the three wings. As thrust coefficient is increased, there is a sharp increase in incremental lift for the model with the 64A006 wing. A detailed comparison of afterbody pressure distributions

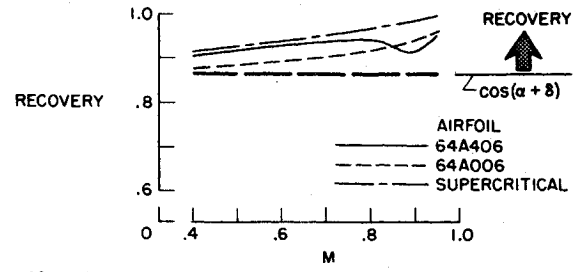

Fig. 13 Effect of Mach number and airfoil variation on thrust recovery. $\delta_d = 30°$, $\alpha + \delta = 30°$ at scheduled pressure ratio.

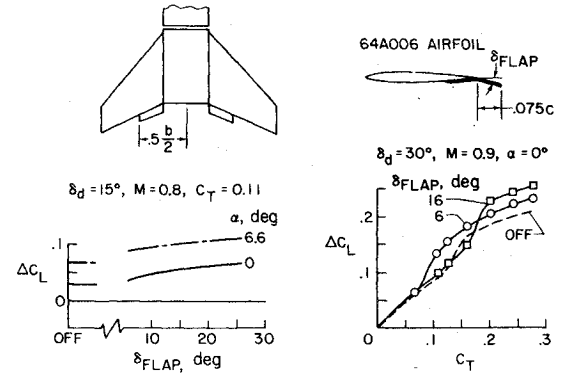

Fig. 14 Effect of trailing-edge flap deflection on incremental lift.

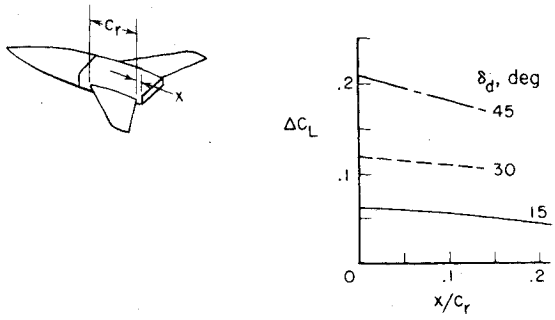

Fig. 15 Effect of varying exit location on incremental lift with 64A406 airfoil. $M = 0.9$, $\alpha = 0°$, $C_T = 0.1$.

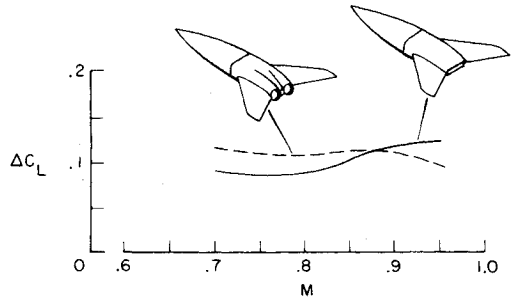

Fig. 16 Effect of nozzle shape on incremental lift with 64A406 airfoil. $\delta_d = 30°$, $\alpha = 0°$ at scheduled pressure ratio.

shows an abrupt rearward movement of the wing shock wave occurring for the 64A006 wing at thrust coefficient near 0.15. It is felt that with the rearward shock movement, a smaller region of the wing is affected by flow separation and hence more lift is generated.

Drag and Thrust Recovery

Variation of incremental drag coefficient ΔC_D with lift coefficient for the three wings at $M = 0.70$ is shown in Fig. 12. Of the three wings, the supercritical showed the greatest drag reduction. An analysis of the drag-due-to-lift characteristics for the supercritical wing (by method of Ref. 4) with the 30° nozzle showed reductions in drag-due-to-lift occurring for most test conditions, whereas similar reductions were previously noted to occur only for the 64A406 wing with the 45° nozzle.

This reduction in drag-due-to-lift for the supercritical wing is probably also due to improved leading-edge suction and may be occurring at a lower nozzle deflection angle because of the basic difference in the type of flow over the top of the airfoil. With the region of accelerated flow over the top reduced because of the flatness of the airfoil, it is now possible for the deflected jet to influence flow completely around the supercritical airfoil.

The variation of drag coefficient with Mach number at constant lift coefficient for the scheduled pressure ratio is also shown in Fig. 12. The poorer drag rise characteristics for the 64A406 wing may be attributed to a higher afterbody drag than for the other airfoils in combination with the afterbody. Thrust recovery characteristics for the three wings are summarized in Fig. 13 at $\alpha + \delta = 30°$ at the scheduled pressure ratio. In general, thrust recovery increases with increasing Mach number and the thrust recovery characteristics of the supercritical airfoil are better than the 64 series airfoils.

Effect of Trailing-Edge Flaps

Simple flaps were tested on the model with the 64A006 airfoil as shown in the upper portion of Fig. 14. This type of flap was chosen in order to get a preliminary indication of flap effectiveness. Typical results are shown in the lower left of Fig. 14 at $M = 0.80$, $\delta_d = 15°$, and $C_T = 0.11$. The wing was not tested with the flap at 0°. Therefore for reference, the flap-off ΔC_L is shown as tick marks on the ordinate. The data have been reduced with the same reference area even though there is a small increase in area with the flaps. In general, increasing flap angle at constant thrust coefficient increases incremental lift ΔC_L at angles of attack up to 6.6°. Similar results were obtained with the 0° and 30° nozzles.

The importance of the interaction of the flowfield imposed by the flap on that of the wing in combination with the deflected jet is illustrated in the right-hand side of Fig. 14. As is the case with the plain wing, combinations of flap deflection and thrust coefficient can affect the location of the wing shock and as shown can result in an abrupt change in incremental lift. Similar results were found at $M = 0.80$.

Effect of Nozzle Exit Location

Nozzle exit location was varied aft from the wing trailing edge from 0% to 21% of the wing root chord (x/c_r). The configurations tested are shown in Table 1. Some typical results at $M = 0.90$ and $\alpha = 0°$ are shown in Fig. 15 where incremental lift is shown as a function of exit location. As would be expected, there is a decrease in incremental lift as the exit is moved aft. The data at all Mach numbers indicate that the percent decrease in incremental lift is a function of nozzle deflection angle, and as deflection angle increases more incremental lift is lost due to a decrease in jet-induced lift. Drag and thrust recovery characteristics are essentially unchanged.

Effect of Nozzle Shape

Circular nozzles with deflection angles of 0° and 30° were investigated with the 64A406 wing. These nozzles also had turning vanes with the nozzle exit located at the wing trailing edge. A comparison of the lift characteristics of the model with round and rectangular exits is summarized in Fig. 16 where incremental lift is shown as a function of Mach number at the scheduled pressure ratio. As can be seen, more lift is generated by the round nozzles up to $M = 0.875$. The results are essentially the same at angle of attack. Since jet lift is approximately the same for both nozzles, the diffences are due primarily to jet-induced supercirculation lift.

Although there is no positive explanation for these results, it is quite possible that the two circular jets are coalescing to form a jet that is somewhat rectangular and thicker than the original rectangular jet and one that behaves similar to it in inducing lift. Even though the lift augmentation characteristics of the round nozzles were comparable with the rectangular exits, the round exits exhibited much poorer thrust recovery characteristics. These poor thrust recovery characteristics are probably due to adverse interference effects of the afterbody.

Conclusions

The current assessment of the potential performance of a wing trailing edge jet-vectoring system indicates several general characteristics. Thrust vectoring results in significant increases in lift, due to supercirculation (gain factors up to 4) and significant drag reduction (thrust recovery maintained to a lift coefficient of 0.5). This lift and drag performance was generally maintained up to a Mach number of 0.9 and to angles of attack where flow separation effects dominate. Variations in configuration geometry indicated that: a) airfoil camber had little effect on the lift and drag performance of the system with a supercritical airfoil shape having significantly better performance; b) locating the jet aft of the wing trailing edge resulted in only a small lift loss; and c) the configuration with round exits had similar lift performance but poorer thurst recovery characteristics than the configuration with rectangular exits.

References

[1] Corson, B. W., Jr., Capone, F. J., and Putnam, L. E., "Lift Induced on a Swept Wing by a Two-Dimensional Partial-Span Deflected Jet at Mach Numbers From 0.20 to 1.30," TM X-2309, 1971, NASA.

[2] Capone, F. J., "Exploratory Investigation of Lift Induced on a Swept Wing by a Two-Dimensional Partial-Span Deflected Jet at Mach Numbers From 0.20 to 1.30," TM X-2529, 1972, NASA.

[3] Corson, B.W., Jr., Runckel, J.F., and Igoe, W.B., "The 16-Foot Transonic Tunnel Calibration with Test Section Air Removal," TR R-423, Aug. 1974, NASA.

[4] Igoe, W. B., Re, R. J., and Cassetti, M. D., "Transonic Aerodynamic Characteristics of a Wing-Body Combination Having a 52.50° Sweptback Wing of Aspect Ratio 3 with Conical Camber and Designed for a Mach Number of $\sqrt{2}$," TN D-817, 1961, NASA.

[5] Lowry, J. G., Riebe, J. M., and Campbell, John P., "The Jet-Augmented Flap," Preprint No. 715, Jan. 1957, S.M.F. Fund Paper, Institute of Aeronautical Sciences, New York.

[6] Williams, J., Butler, S.F.J., and Ward, M. N., "The Aerodynamics of Jet Flaps," R. and M. No. 3304, British Aeronautical Research Council, London, Jan. 1963.

[7] Maskell, E. C., and Spence, D. A., "A Theory of the Jet Flap in Three Dimensions," *Proceedings of the Royal Society (London): Ser. A, Mathematical and Physical Sciences*, Vol. 251, June 1959, pp. 407-425.